Thermal resilience of microcracked andesitic dome rocks

Michael J. Heap[1]*, Rebecca Coats[2], Chong-feng Chen[3,4], Nick Varley[5], Yan Lavallée[2], Jackie Kendrick[2], Tao Xu[3,4], Thierry Reuschlé[1]

[1]*Géophysique Expérimentale, Institut de Physique de Globe de Strasbourg (UMR 7516 CNRS, Université de Strasbourg/EOST), 5 rue René Descartes, 67084 Strasbourg cedex, France*

[2]*Earth, Ocean and Ecological Sciences, University of Liverpool, Liverpool L69 3GP, United Kingdom*

[3]*Key Laboratory of Ministry of Education on Safe Mining of Deep Metal Mines, Northeastern University, Shenyang, 110819, P. R. China*

[4]*Center for Rock Instability and Seismicity Research, Northeastern University, Shenyang 110819, P. R. China*

[5]*Facultad de Ciencias, Universidad de Colima, Las Víboras, Colima, Mexico*

*Corresponding author: Michael Heap (heap@unistra.fr)

Highlights

- Physical properties of andesite unaffected by transient exposure to high temperature.
- Physical properties of andesite unaffected by shock-cooling.
- Strength and stiffness of andesite increases when deformed at high temperature.
- Thermal perturbations may not reduce dome stability

Abstract

The strength of the rocks forming a lava dome informs on its structural stability, important for volcanic hazard assessments. Dome-forming rocks are persistently challenged by thermal stresses from recurring eruptive events that may reduce their strength and jeopardise the structural stability of the dome. Here, we present a series of experiments to better understand the impact of thermal stresses on the strength of an andesitic dome rock from Volcán de Colima (Mexico), a volcano that has witnessed some substantial dome collapses in recent years. Uniaxial compressive strength (UCS) was first tested at room temperature on as-collected samples and samples that had undergone either slow (heated and cooled at 1 °C/min) or shock (heated at 1 °C/min and shock-cooled in cold water) thermal stressing to target temperatures of 400-700 °C. Slow- and shock-cooling thermal stressing did not measurably alter the strength, connected porosity, or permeability. UCS tests performed at high *in-situ* temperatures (400-700 °C), however, showed an increase in sample strength and stiffness. We interpret that the resistance of this rock to thermal stresses results from both the presence of abundant pre-existing microcracks and the thermal stability of its mineral assemblage. Unchanged physical properties for the thermally stressed samples deformed at room temperature suggests that the pre-existing microcracks close and reopen, respectively, as the rock expands and contracts during heating and cooling to accommodate the volumetric changes without further microcracking. The increase in strength and stiffness at high *in-situ* temperatures can be explained by the closure of microcracks due to thermal expansion. These observations suggest that the strength of microcracked dome rocks (1) may be slightly higher when hot (below the glass transition of the groundmass glass), although "upscaled" strength estimates highlight that dome strength will be largely unchanged by an increase in temperature, (2) may only be reduced following the first thermal stressing event, and (3) may not be further reduced by repeated thermal stressing events. Therefore, thermal perturbations, often

observed at active domes, may not, as perhaps expected, repeatedly degrade the strength of individual blocks forming the lava dome and therefore not jeopardise dome stability.

Keywords: Strength; porosity; permeability; elastic modulus

1 Introduction

Lava dome collapses can result in potentially dangerous block-and-ash flow avalanches and trigger explosive volcanic behaviour (e.g., Cole et al., 1998; Calder et al., 2002; Voight et al., 2006; Loughlin et al., 2010). The structural integrity of a lava dome therefore forms an important component of volcanic hazard assessment (e.g., Sparks, 1997; Voight, 2000; Voight and Elsworth, 2000; James and Varley, 2012; Ball et al., 2013; Calder et al., 2015; Ogburn et al., 2015; Ball et al., 2015; Harnett et al., 2018). Dome collapse events at Volcán de Colima (Mexico), for example, regularly produce dangerous pyroclastic density currents (e.g., one reached 6.1 km from the vent in 2004 and 10.6 km in 2015; Varley et al., 2018). Here, as at many stratovolcanoes, this represents the most frequent high-risk scenario for the local population.

The rocks forming the outermost part of the dome (the talus) on an active volcano may be repeatedly challenged by thermal stresses generated by the influx of hot magma into the viscous core of the dome, and by hydrothermal fluids migrating through the dome (e.g., Oppenheimer et al., 1993; Wooster and Kaneko, 1998; Dehn et al., 2000; Kaneko et al., 2002; Carter et al., 2007; Sahetapy-Engel et al., 2008; Stevenson and Varley, 2008; Sahetapy-Engel and Harris, 2009; Bernstein et al., 2013; Hutchinson et al., 2013). As an example, we provide here airborne thermal images of the active dome at Volcán de Colima between 2013 and 2016 (Figure 1), taken using a Jenoptic VarioCAM hr thermal camera (see Hutchinson et al. (2013) for technical specifications). These images, which show a variety of slow- and fast-extruding lava (some of which

overflowed to form a lava flow), highlight that the apparent temperature of exposed talus rocks can vary significantly in time and space (Figure 1) and can reach temperatures of almost 700 °C (Figure 1h). Although the highest temperature is associated with the highest effusion rate (Figure 1h), no discernable trend exists between maximum temperature and effusion rate for the examples shown in Figure 1. Hutchinson et al. (2013) monitored the surface temperature of the talus rocks at Volcán de Colima over a three-year period, from 2007 to 2010. These data show that the surface temperature of the dome top was reduced from ~350 to ~200 °C in 2007 as the freshly exposed rocks cooled, after which the temperature fluctuated from ~150 to ~250 °C until mid-2009 when it increased to ~300 °C due to the initiation of a new lobe; the maximum temperature of the lobe reached ~400 °C (Hutchinson et al., 2013). Increases and decreases in temperature are known to result in thermal microcracking of rocks (e.g., Fredrich and Wong, 1986; Homand and Houpert, 1989; David et al., 1999; Browning et al., 2016; Griffiths et al., 2018), which can reduce their strength (e.g., Kranz, 1983; David et al., 2012; Griffiths et al., 2017). Further, experiments have also shown that more microcracks, and greater changes to rock physical properties, are observed at higher rates of heating/cooling (e.g., Yong and Wang, 1980). The repeated, and often rapid, thermal stressing of the talus rocks could therefore reduce the overall strength of the dome and increase the likelihood of potentially devastating dome collapses.

The influence of transient exposure to high temperature on the microstructure and therefore strength of volcanic rocks is unclear at present. For example, the strength of andesites from Volcán de Colima was unchanged following exposure to 450 °C (Heap et al., 2014). Similar results were found for dacites from Mt. St. Helens (USA) (heated up to 900 °C; Kendrick et al., 2013) and Mt Unzen (Japan) (heated up to 900 °C; Coats et al., 2018), and basalts from Pacaya volcano (Guatemala) (heated up to 935 °C; Schaefer et al., 2015) and Krafla volcano (Iceland) (heated up to 450 °C; Eggertsson et al., 2018). On the other hand, the strength of high-porosity tuff was greatly reduced following

exposure to high temperature (heated up to 1000 °C; Heap et al., 2012; 2018). Further, the studies listed above used slow heating/cooling rates (1-4 °C/min) to minimise the influence of microcracking due to high thermal gradients. However, thermal gradients in volcanic environments are expected to greatly exceed these heating/cooling rates. For example, heavy rainfall on hot dome rocks can rapidly reduce their temperature (e.g., Elsworth et al., 2004; Matthews and Barclay, 2004) by more than 100 °C within a few minutes (i.e. "shock-cooling"; Matthews and Barclay, 2004). Many active stratovolcanoes are located in climates associated with heavy seasonal rainfall. For example, Volcán de Colima exists within a tropical savanna climate with consistently high temperatures and pronounced dry (November to May) and wet seasons (June to October). We provide here rainfall data (from January 2001 to December 2003) obtained from permanent meteorological monitoring stations that form part of the CONAGUA (Comisión Nacional del Agua) network. The three closest stations were chosen, located in the towns of Cuauhtémoc, Comala, and Minatitlán (at a distance of 19, 24, and 47 km from the vent of the volcano, respectively; Figure 2a). The data show that there is no rainfall, or only a few mm of rain, from November to May, and that there is often several hundred mm of rainfall per month between June and October (Figure 2b). In August 2001 there was almost 500 mm of rain in the town of Cuauhtémoc (Figure 2b). High cooling rates are also experienced by dome rocks emplaced subaqueously, which are typically highly fractured as a result (e.g., Smellie et al., 1998). However, few experimental studies have used the high thermal gradients likely experienced by the talus rocks. Experimental studies designed to better understand the influence of shock-cooling on the physical properties of volcanic rocks have shown, for example, that the shock-cooling (quenching) of basalt (from Lyttelton volcano, New Zealand) in water resulted in higher values of porosity and permeability compared with those cooled slowly (Siratovich et al., 2015). Eggertsson et al. (2018) found that shock-cooling only affected the physical properties of volcanic rocks from Krafla volcano (Iceland) if they were originally devoid

of microcracks. However, our knowledge on the influence of shock-cooling on the physical properties of volcanic rocks is still embryonic.

The strength of volcanic rocks is often measured at room temperature (e.g., Al-Harthi et al., 1999; Loaiza et al., 2012; Adelinet et al., 2013; Kendrick et al., 2013; Heap et al., 2014; Zhu et al., 2016; Zorn et al., 2018). At high *in-situ* temperatures (i.e. experiments in which the rocks were deformed at high-temperature), the strength of volcanic rocks (crystallised or below the glass transition of their groundmass glass) has been measured to be more-or-less the same as the strength at room temperature (e.g., Bauer et al., 1981; Smith et al., 2009; 2011) or to increase with increasing temperature (e.g., Duclos and Paquet, 1991; Schaefer et al., 2015; Heap et al., 2017a; Coats et al., 2018). In the case of a basalt from Mount Etna (Italy), no strength changes were observed up to 900 °C, but, at 950 °C, the rock was stronger and Young's modulus lower (Benson et al., 2012). A recent study found that the strength and Young's modulus of a basalt with a low fracture density from Selljavellir (Eyjafjallajökull volcano, Iceland) increased from ambient (room) temperature to 900 °C (Lamur et al., 2018). Despite these studies, most high-temperature deformation experiments on volcanic materials typically target temperatures at which the groundmass glass can deform viscously (e.g., Cordonnier et al., 2009; Lavallée et al., 2007; 2013), experiments highly relevant to understand the conduit-dwelling magma and the viscous core of a lava dome. However, a paucity of data still exists for the strength of volcanic rock at temperatures more representative of the cooler talus rocks (< 700 °C). Because it is the cooled talus rocks that are able to construct precarious dome structures, such as lava spines (e.g., Watts et al., 2002), the strength of the talus rocks is therefore an important factor in dictating their collapse.

To better understand the influence of high and fluctuating temperatures (increases in temperature due to the influx of hot magma into the ductile core of the dome and the migration of hot fluids, and decreases in temperature due to, for example,

rainfall) on a typical dome rock, we present herein a systematic laboratory study in which we first measured the strength of an andesite from Volcán de Colima transiently exposed to high temperatures and deformed at room temperature and then at high *in-situ* temperatures. Strength measurements are first performed on samples that have been thermally-stressed to different target temperatures (from 400 to 700 °C, a reasonable temperature range for dome rocks; Figure 1) and cooled at different rates (slow- and shock-cooled). We then performed strength measurements at high *in-situ* temperatures (from 400 to 700 °C). Finally, we use our experimental data to explore the influence of temperature on the "upscaled" strength of a dome, using the generalised Hoek-Brown failure criterion (Hoek et al., 2002).

2 Experimental material and methods

The rock chosen for this study was an andesite collected from the El Zarco ravine on the south-eastern flank of Volcán de Colima (the same block of material used in Farquharson et al., 2016a). Its precise eruptive origin cannot be specified, since rather than being collected *in-situ*, it has been remobilised by pyroclastic density currents and/or lahars within the ravine. Volcán de Colima is an active andesitic stratovolcano located at the western end of the Trans-Mexican Volcanic Belt, Mexico (Figure 2a; Lavallée et al., 2012; Varley et al., 2018). Although our block was sourced from one particular volcano, we consider the implications presented in this study to be applicable to active and frequently collapsing stratovolcanoes worldwide. Indeed, rocks with very similar microstructures have been seen at, for example, Mt. Ruapehu (New Zealand; Heap and Kennedy, 2016) and Mt. Merapi (Indonesia; Kushnir et al., 2016). The andesite collected has a porphyritic texture consisting of a microlitic groundmass (that contains little glass) that hosts a phenocryst cargo (predominantly plagioclase with subordinate orthopyroxene and clinopyroxene) (Figure 3). Porosity within the sample comprises of the volume between microlites where the groundmass is absent (diktytaxitic texture;

187 Figures 3a and 3c) and long and tortuous microcracks (Figure 3b). Microcracks are seen
188 to traverse through the groundmass and the phenocrysts (Figure 3b).

189 Cylindrical samples (20 mm in diameter and nominally 40 mm in length) were
190 all cored from the block, in the same orientation, and precision-ground such that their
191 end faces were flat and parallel. Once prepared, these samples were washed and then
192 allowed to dry in a vacuum oven at 40 °C for at least 48 h. Their connected porosities
193 were determined using the connected (skeletal) volume measured by a helium
194 pycnometer (Micromeritics AccuPyc II 1340) and the bulk volume calculated using the
195 sample dimensions.

196 First, three samples of the oven-dried as-collected material (i.e. material that has
197 undergone no laboratory thermal stressing: "as-collected") were deformed in the
198 uniaxial "Schenk" loadframe at the University of Strasbourg (see Heap et al. (2014) for a
199 schematic of the experimental device). These samples were deformed at room
200 temperature and at a constant strain rate of 10^{-5} s^{-1} until macroscopic failure (i.e.
201 following the stress drop associated with the formation of a system-lengthscale
202 fracture). A lubricating wax was applied to the end-faces of the dry samples to avoid
203 problems associated with the friction between the sample and the pistons. During
204 deformation, axial displacement and axial load were measured using a linear variable
205 differential transducer (LVDT) and a load cell, respectively. These measurements were
206 converted to axial strain and axial stress using the sample dimensions. The
207 displacement measured was corrected to subtract the displacement of the load chain.
208 The static elastic modulus was determined for each experiment from the elastic portion
209 of the stress-strain curves.

210 Sixteen samples were thermally stressed to target temperatures of 400, 500,
211 600, or 700 °C at a constant heating rate of 1 °C/min (four samples per target
212 temperature). Temperatures ≤ 700 °C are considered here to be below the glass
213 transition temperature of the groundmass glass (Lavallée et al., 2013; Heap et al.,

2017a). The samples were left at the target temperature for two hours to ensure thermal equilibrium. Eight of the samples were cooled back to room temperature at a cooling rate of 1 °C/min and the other eight were shock-cooled by placing them directly in a bath of cold water. These samples returned to room temperature in a matter of seconds, equating to cooling rates on the order of 100 °C/s. The shock-cooled samples were dried in a vacuum oven at 40 °C for at least 48 h. The connected porosities of all sixteen samples were remeasured (as explained above). To explore the time constant, t, required for the thermal equilibration of a cylindrical core sample, we measured the thermal diffusivity, d, of the studied andesite using the Hot Disk TPS 500 Thermal Constants Analyser at the University of Strasbourg (see Heap et al., 2018 for details of operational procedure). The time constant, t, required for the thermal equilibration is given by $t = r^2/d$, where r is the sample radius (1×10^{-2} m for our samples). The thermal diffusivity was measured to be 0.67957 ± 0.026316 mm^2/s, yielding a time constant of about 150 s. Therefore, our imposed heating/cooling rates of 1 °C/min and ~100 °C/s were, respectively, very close to and very far from the a heating/cooling rate that allows for complete thermal equilibration of the sample. The permeability of the sixteen thermally stressed samples was measured using a nitrogen gas benchtop permeameter at the University of Strasbourg (Farquharson et al., 2016b; Heap and Kennedy, 2016) under a confining pressure of 1 MPa (required to ensure that gas does not pass between the sample and the rubber jacket). Due to their low permeability, all samples were measured using the pulse-decay method (Brace et al., 1968). Prior to measurement, samples were left at 1 MPa for 1 hour to allow for microstructural equilibration. We also assessed the need for the Klinkenberg and Forchheimer corrections, which were applied on a case-by-case basis. For the samples measured herein, the Klinkenberg correction was required in each case. The pulse-decay procedure used here is outlined in detail in Heap et al. (2017b). These samples were

240 then deformed uniaxially at a constant strain rate of 10^{-5} s^{-1} until macroscopic failure,
241 using the method described above.

242 Eight high temperature uniaxial compressive strength tests were carried out
243 using a 100 kN 1362 Instron uniaxial press (8862 load frame) in the Experimental
244 Volcanology and Geothermal Research Laboratory at the University of Liverpool (as
245 described in Coats et al., 2018). The press is equipped with a three–zone, split cylinder
246 furnace to allow experiments to be performed at high-temperature. The samples were
247 heated to the target temperature at a rate of 1 °C/min and were left at the target
248 temperature for > 1 h to achieve thermal equilibrium with the pistons. The bottom
249 piston was then raised such that both pistons were in contact with the sample. Once the
250 target temperature was reached and stabilised, the sample was deformed until
251 macroscopic failure (set as a stress drop exceeding 20% of the monitored peak stress
252 achieved). The samples were deformed at a constant strain rate of 10^{-5} s^{-1} until
253 macroscopic failure at constant *in-situ* temperatures of 400, 500, 600, and 700 °C (two
254 samples per target temperature). The press monitored the applied load (with a 2527
255 series Dynacell Load cell at an accuracy better than 0.25% down to 1% of the load cell
256 full scale) and piston displacement via a LVDT within the electric actuator, which were
257 converted to axial stress and axial strain using the sample dimensions. All of the
258 mechanical data were corrected for the compliance of the setup at each temperature.
259 The static elastic modulus was determined for each experiment from the elastic portion
260 of the stress-strain curves.

261 The linear thermal expansion coefficient (α) of the rock was measured using a
262 Netzsch TMA 402 F1 Hyperion Thermo-mechanical Analyser (TMA) at the University of
263 Liverpool. To accurately quantify the thermal expansivity of the rock, we first performed
264 a baseline measurement to determine the expansivity of the sample assembly by loading
265 a cylinder of alumina (6.0 mm diameter by 5.0 mm-long) between the two pistons of the
266 TMA, and heating at a rate of 2 °C/min up to 950 °C, whilst applying an axial load of 10

mN and monitoring length change at a spatial resolution of 0.125 nm; upon reaching temperature, the sample was left to dwell for 1 h before cooling at the same rate. Then the thermal expansion of a rock sample of equal dimension (within 5%) to that of the alumina standard was measured under the same thermal and load history. Following these measurements, the baseline was subtracted from the sample run to obtain the corrected sample length change as a function of temperature and thus determine the linear thermal expansion coefficient of the sample.

3 Results

The stress-strain curves for the three as-collected samples are shown in Figure 4a. These stress-strain curves are typical of those for brittle rock in compression (e.g., Hoek and Bieniawski, 1965; Brace et al., 1966; Scholz, 1968). The three curves in Figure 4a highlight that the strength of the as-collected material can vary by up to 20 MPa over a relatively small porosity range (data available in Table 1). The stress-strain curves for the slow-cooled and shock-cooled samples are provided in Figures 4b and 4c, respectively. The stress-strain curves in Figures 4b and 4c show that there is essentially no difference in the mechanical behaviour and the strength between the samples slow- and shock-cooled to temperatures between 400 and 700 °C (Figures 4b and 4c) and the as-collected material (Figure 4a).

Uniaxial compressive strength, static elastic modulus, and permeability are plotted as a function of thermal-stressing temperature in Figures 5a, 5b, and 5c, respectively. Each plot contains as-collected data (white circles), as well as data for the slow-cooled (grey circles) and shock-cooled (black circles) samples (data available in Table 1). The data of Figure 5 show that slow- and shock-cooling did not change the uniaxial compressive strength, elastic modulus, or permeability of the andesite. We also note that the change in the connected porosity of the samples following thermal-

293 stressing (slow- and shock-cooled) is within the standard deviation of the measurement
294 (Table 1).

295 The stress-strain curves for the samples deformed at high *in-situ* temperatures
296 are shown in Figure 4d. These data show that there appears to be an increase (of about
297 15% from room temperature to 700 °C) in the strength of the andesite at high-
298 temperature. The strengths of the samples tested at 400 °C (black curves on Figure 4d),
299 for example, are noticeably lower than those tested at higher temperatures (grey to light
300 grey curves on Figure 4d). Uniaxial compressive strength and static elastic modulus are
301 plotted as a function of the testing temperature in Figures 6a and 6b, respectively. Each
302 plot contains as-collected data (white circles) as well as data for the samples deformed
303 at high *in-situ* temperatures (red circles) (data available in Table 2). The data of Figure 6
304 show that there appears to be an increase in uniaxial compressive strength (Figure 6a)
305 and static elastic modulus with increasing testing temperature (Figure 6b).

306 The results of our thermal expansivity measurement, axial strain and the
307 thermal expansion coefficient, are plotted as a function of temperature in Figure 7. Our
308 data show that axial strain increases (i.e. the sample is expanding) linearly with
309 temperature, up to a value of $\sim 1 \times 10^{-2}$ at the maximum temperature of 950 °C (Figure
310 7). The thermal expansion coefficient does not vary significantly or systematically with
311 temperature (Figure 7). The average thermal expansion coefficient for the studied
312 andesite was measured to be $\sim 1 \times 10^{-5}$ °C^{-1} (Figure 7).

313

314 **4 Discussion**

315

316 4.1 Influence of thermal-stressing (slow- and shock-cooling)

317 Our experimental data show that slow- and shock-cooling the studied andesite
318 (up to target temperatures of 700 °C) did not alter the connected porosity, permeability,
319 static elastic modulus, or uniaxial compressive strength (Table 1; Figure 5). A plot of

uniaxial compressive strength as a function of porosity for as-collected (from this study and Heap et al., 2014, 2015; white circles), slow-cooled (from this study and Heap et al., 2014; grey circles), and shock-cooled (from this study; black circles) for andesites from Volcán de Colima are shown in Figure 8. Given the sample-to-sample variability of volcanic rocks, these collated data show that all materials, regardless of their thermal-stressing history, can be described by a single non-linear trend of uniaxial compressive strength-porosity, commonly observed for porous rocks (e.g., Baud et al., 2014).

We interpret the thermal resilience of the studied andesite as a result of the (1) thermal stability of the mineral assemblage (phenocrysts of plagioclase, orthopyroxene, and clinopyroxene within a microlitic groundmass) and (2) the presence of abundant pre-existing microcracks (Figure 3b). First, the studied andesite (Figure 3) does not contain any minerals that would break down at temperatures < 700 °C, such as clays and zeolites (as confirmed by microstructural analyses and the absence of mass losses following exposure to high-temperature). Indeed, the weakening with increasing temperature observed in high-porosity tuffs, for example, was explained by the structural breakdown of clays and zeolites at high temperature (Heap et al., 2012; 2018). Second, the nucleation and growth of thermal microcracks is linked to stresses that arise as the minerals expand and contract as temperature is increased and decreased, respectively. Indeed, thermal microcracking in volcanic rocks has been interpreted to occur during heating and cooling (Heap et al., 2014; Browning et al., 2016). We suggest, herein, that pre-existing microcracks (Figure 3b) close and reopen, respectively, as the rock expands and contracts during heating and cooling to accommodate volumetric changes without further microcracking (as surmised previously by Vinciguerra et al., 2005; Heap et al., 2014; Eggertsson et al., 2018, amongst others). This interpretation is supported by our thermal expansivity data (Figure 7), which not only show that the studied andesite expands with increasing temperature (it is interpreted here that this expansion can close compliant microcracks; e.g., Richter and

Simmons, 1974), but also that the thermal expansivity coefficient remains roughly constant; substantial decreases to this coefficient are expected if thermal microcracks are forming (Cooper and Simmons, 1977). Our observations are therefore consistent with the so-called thermal Kaiser effect (e.g., Heap et al., 2014; Griffiths et al., 2018), whereby no further thermal microcracking occurs within a rock sample until it has been exposed to a temperature higher than it has experienced previously. Indeed, magmatic temperatures, and the temperature within the ductile portion of the dome, at Volcán de Colima are considered to be ≥ 900 °C (e.g., Lavallée et al., 2012; Hutchinson et al., 2013).

4.2 Influence of high *in-situ* temperatures

Our experimental data show that high *in-situ* temperatures increased the uniaxial compressive strength and stiffness (i.e., elastic modulus) of the studied andesite (Table 2; Figures 6 and 8), in line with the experimental observations of Duclos and Paquet (1991), Schaefer et al. (2015), Heap et al. (2017a), and Coats et al. (2018). The increase in sample strength and stiffness with temperature is explained here by the closing/narrowing of microcracks due to the thermal expansion of the mineral constituents, a hypothesis supported by our thermal expansivity data (Figure 7). An increase in the number and/or aperture of microcracks is well known to reduce rock strength and stiffness (e.g., David et al., 2012; Griffiths et al., 2017). We consider microcrack healing unlikely because (1) the target temperature was always below the glass transition of the amorphous glass phase, and (2) solid-state sintering likely requires timescales (weeks to months to years) longer than our experimental timescales (on the order of a couple of hours) and higher pressures (e.g., Ryan et al., 2018).

4.3 Implications for dome stability

The overall strength of a lava dome (i.e., a rock mass) is governed by the strength of the dome-forming materials and the structure (fracture density and fracture

quality) of the dome (e.g., Hoek et al., 2002). Due to the small size of our experimental samples (below the lengthscale of the macrofracture spacing) we therefore provide measurements of the strength of the dome-forming blocks (i.e. the "intact" strength). Laboratory measurements of strength are a vital ingredient in volcanic rock mass strength assessments designed to assess volcanic hazards (e.g., Watters et al., 2000; Thomas and Petford, 2004; Apuani et al., 2005; del Potro and Hürlimann, 2008). Therefore, for a given rock mass structure (fracture density and fracture surface condition), our results suggest that an increase in temperature will slightly increase the strength of the dome (below the glass transition of the groundmass glass; Figure 6a).

We can use the generalised Hoek-Brown failure criterion (Hoek et al., 2002) to estimate the influence of high-temperature on the strength of a dome (i.e. the "upscaled" rock mass):

$$\sigma_1 = \sigma_3 + C_o \left(m_b \frac{\sigma_3'}{C_o} + s \right)^a \quad (1)$$

where C_o is the uniaxial strength of the intact material, σ_1 and σ_3 are the greatest and least principal stress, respectively, and m_b, s, and a are unitless fitting parameters for a fractured rock mass that are defined as follows (Hoek et al., 2002):

$$m_b = m_i \, e^{\left(\frac{GSI-100}{28-14D}\right)} \quad (2)$$

$$s = e^{\left(\frac{GSI-100}{9-3D}\right)} \quad (3)$$

$$a = \frac{1}{2} + \frac{1}{6}\left(e^{-\frac{GSI}{15}} + e^{\frac{-20}{3}}\right) \quad (4)$$

where D is a unitless disturbance factor related to blasting damage in large excavations (we therefore let D = 0 in our analysis; we provide the full equation here for

395 completeness) and GSI is the Geological Strength Index, a unitless value that describes
396 the rock mass characteristics (Marinos et al., 2005). The GSI is a number from 0 to 100,
397 where 0 would represent an essentially cohesionless rock mass and 100 would
398 represent a pristine (fracture-free) rock mass (Marinos et al., 2005). Since volcanic rock
399 masses are typically fractured, estimates of their GSI have been found within the range
400 40-85 (Watters et al., 2000; Okubo, 2004; Thomas et al., 2004; Moon et al., 2005; Apuani
401 et al., 2005a, 2005b; del Potro and Hürlimann, 2008 and references therein). Indeed, the
402 dome at Volcán de Colima is highly fractured (e.g., Kolzenburg et al., 2012; Farquharson
403 et al., 2016b; Kendrick et al., 2016). In our analysis, we will let GSI = 50. The unitless
404 constant m_i describes the shape of the failure envelope on a graph of σ_1 as a function of
405 σ_3, and is therefore related to the microstructural and mineralogical attributes of the
406 rock (mineral content, grain size, grain shape, pore size, and pore shape, amongst many
407 others) (Eberhardt, 2012). In the absence of triaxial data for the andesite studied herein,
408 we use the m_i estimate for andesite (m_i = 19) given in Hoek and Brown (1997). Finally,
409 since we are interested in the strength of the dome, we let σ_3 = 0 MPa. If we use 110 and
410 130 MPa to represent the strength (i.e. C_o) of the talus rocks at 20 and 700 °C,
411 respectively (Tables 1 and 2), we arrive at upscaled dome strengths of 6.6 and 7.8 MPa,
412 respectively. Although these estimates assume a single rock type and that the
413 underlying viscous core does not influence dome strength, our simple analysis suggests
414 that the strength of a lava dome is largely governed by its structure or physical state
415 (fracture density and fracture surface condition), rather than the strength of the
416 individual blocks. We conclude that, although temperature increases the strength of the
417 talus rocks on the sample lengthscale (Figure 6a), an increase in temperature will not
418 significantly change the strength of a lava dome on the rock mass scale. However, we
419 also note that the thermal expansion of the rocks forming the talus could result in
420 instability. For example, Mueller et al. (2013) show that rockfall volume correlates well

421 with the surface temperature of the freshly exposed dome surface, highlighting that
422 larger thermal perturbations could be responsible for dislodging larger dome blocks.

423 Our results also suggest that exposure to high-temperature perturbations,
424 following the first thermal stressing event, will not influence the strength (Figure 5a) or
425 permeability (Figure 5c) of the dome rock. Further, shock-cooling of dome rocks due to,
426 for example, heavy rainfall (see Figure 2) will also not influence the physical properties
427 of the dome rock (Figure 5), although dome instability in this scenario will be much
428 more dependent on pore pressure build-up between dome fractures (i.e. between
429 individual blocks) (Elsworth et al., 2004). Based on our experimental observations we
430 conclude that thermal perturbations, often observed at active domes (Figure 1), may
431 not, as perhaps expected, repeatedly degrade the strength of individual blocks forming
432 the lava dome and therefore jeopardise dome stability.

433 The thermal resilience of the dome rock studied herein is likely due to (1) the
434 pre-existing microcrack population: dome rocks with lower microcrack densities or
435 different microstructures may be affected differently (at least during the first thermal
436 perturbation) (see Heap et al. (2014) and Eggertsson et al. (2018) for further
437 discussion) and (2) due to the thermal stability of its mineral phases: dome rocks that
438 are heavily altered by hydrothermal processes may contain carbonates, clays, and/or
439 zeolites, for example, that will devolatilise at high temperature thereby increasing
440 porosity and potentially decreasing dome strength. Finally, although we flag the
441 potential importance of porosity type (pores versus microcracks) on the thermal
442 response of a dome rock (see also Eggertsson et al., 2018), the influence of porosity or
443 glass content on the thermal microcracking process is still unclear. However, data from
444 Heap et al. (2017a) show that the porosity, permeability, and P-wave velocity of porous
445 (large pores and microcracks; porosity = 0.265) andesite is unaffected by transient (2 h)
446 exposure to temperatures up to 900 °C. A complete understanding of thermal
447 microcracking in volcanic rocks is a challenging prospect due to their complex and

varied microstructures (e.g., Shea et al., 2010; Farquharson et al., 2015; Colombier et al., 2017). We recommend that future studies focus on the influence of high temperature on the strength of altered dome rocks, which may be more susceptible to exposure to high temperature.

5 Concluding remarks

The rocks forming a lava dome are persistently challenged by temperature perturbations that could influence their strength and affect dome stability. Our experimental study on a microcracked andesite from Volcán de Colima shows that strength is unaffected by transient (a couple of hours) exposure to high temperature and by rapid cooling (quenching). Experiments, however, also show that the strength of the andesite is higher at higher *in-situ* temperatures, although "upscaled" strength estimates highlight that dome strength will be largely unchanged by an increase in temperature. We interpret these experimental observations as a result of the (1) thermal stability of the mineral assemblage at the examined temperature range (<700 °C) and (2) the presence of abundant pre-existing microcracks that accommodate (by closing and opening) volume changes during heating and cooling. We conclude that thermal perturbations, often observed at active domes, may not repeatedly degrade the strength of individual blocks forming the lava dome and therefore do not jeopardise dome stability. However, we highlight that hydrothermally altered dome rocks (such as those at, for example, La Soufrière de Guadeloupe (Rosas-Carbajal et al., 2016) and Mt. Merapi (Byrdina et al., 2017)) that contain minerals such as clays may weaken when exposed to high temperatures and reduce dome stability, offering an inviting avenue for future research.

Acknowledgements

This work was made possible by a Partenariats Hubert Curien (PHC) Cai Yuanpei

grant (grant number 36605ZB). We are grateful to Bertrand Renaudié for preparing the samples. We additionally thank Jamie Farquharson, Alexandra Kushnir, and Paul Anthony Wallace for experimental support. Gilles Morvan is thanked for SEM assistance. Conversations with Marlène Villeneuve inspired elements of this work. The support provided by the Natural Science Foundation of China (Grant Nos. 51474051 and 41672301), the National Basic Research Program (973) of China (Grant No. 2014CB047100), and the Fundamental Research Funds for the Central Universities of China (N150102002) are highly acknowledged. We also acknowledge funding from the European Research Council (ERC) Starting Grant SLiM (Strain Localisation in Magma; No. 306488). An Early Career Fellowship of the Leverhulme Trust supported Jackie E. Kendrick. We're thankful for the helpful comments of two anonymous reviewers.

References

Adelinet, M., Fortin, J., Schubnel, A., & Guéguen, Y. (2013). Deformation modes in an Icelandic basalt: from brittle failure to localized deformation bands. *Journal of Volcanology and Geothermal Research*, *255*, 15-25.

Al-Harthi, A. A., Al-Amri, R. M., & Shehata, W. M. (1999). The porosity and engineering properties of vesicular basalt in Saudi Arabia. *Engineering Geology*, *54*(3-4), 313-320.

Apuani, T., Corazzato, C., Cancelli, A., & Tibaldi, A. (2005a). Physical and mechanical properties of rock masses at Stromboli: a dataset for volcano instability evaluation. *Bulletin of Engineering Geology and the Environment*, *64*(4), 419.

Apuani, T., Corazzato, C., Cancelli, A., & Tibaldi, A. (2005b). Stability of a collapsing volcano (Stromboli, Italy): Limit equilibrium analysis and numerical modelling. *Journal of Volcanology and Geothermal Research*, *144*(1-4), 191-210.

Ball, J. L., Calder, E. S., Hubbard, B. E., & Bernstein, M. L. (2013). An assessment of hydrothermal alteration in the Santiaguito lava dome complex, Guatemala: implications for dome collapse hazards. *Bulletin of Volcanology*, *75*(1), 676.

Ball, J. L., Stauffer, P. H., Calder, E. S., & Valentine, G. A. (2015). The hydrothermal alteration of cooling lava domes. Bulletin of Volcanology, 77(12), 102.

Bauer, S. J., Friedman, M., & Handin, J. (1981). Effects of water-saturation on strength and ductility of three igneous rocks at effective pressures to 50 MPa and temperatures to partial melting (No. DOE/ER/10361-T2). Texas A and M Univ., College Station (USA). Center for Tectonophysics.

Benson, P. M., Heap, M. J., Lavallée, Y., Flaws, A., Hess, K. U., Selvadurai, A. P. S., ... & Schillinger, B. (2012). Laboratory simulations of tensile fracture development in a volcanic conduit via cyclic magma pressurisation. *Earth and Planetary Science Letters*, *349*, 231-239.

Bernstein, M., Pavez, A., Varley, N., Whelley, P., & Calder, E. S. (2013). Rhyolite lava dome growth styles at Chaitén Volcano, Chile (2008-2009): Interpretation of thermal imagery. *Andean Geology*, *40*(2).

Brace, W. F., Paulding Jr, B. W., & Scholz, C. H. (1966). Dilatancy in the fracture of crystalline rocks. *Journal of geophysical research*, *71*(16), 3939-3953.

Brace, W., Walsh, J. B., & Frangos, W. T. (1968). Permeability of granite under high pressure. *Journal of Geophysical research*, *73*(6), 2225-2236.

Browning, J., Meredith, P., & Gudmundsson, A. (2016). Cooling-dominated cracking in thermally stressed volcanic rocks. *Geophysical Research Letters*, *43*(16), 8417-8425.

Byrdina, S., Friedel, S., Vandemeulebrouck, J., Budi-Santoso, A., Suryanto, W., Rizal, M. H., & Winata, E. (2017). Geophysical image of the hydrothermal system of Merapi volcano. *Journal of Volcanology and Geothermal Research*, *329*, 30-40.

Calder, E. S., Luckett, R., Sparks, R. S. J., & Voight, B. (2002). Mechanisms of lava dome instability and generation of rockfalls and pyroclastic flows at Soufriere Hills Volcano, Montserrat. *Geological Society, London, Memoirs*, *21*(1), 173-190.

Calder, E. S., Lavallée, Y., Kendrick, J. E., & Bernstein, M. (2015). Lava dome eruptions. In The Encyclopedia of Volcanoes (Second Edition) (pp. 343-362).

Carter, A. J., Ramsey, M. S., & Belousov, A. B. (2007). Detection of a new summit crater on Bezymianny Volcano lava dome: satellite and field-based thermal data. *Bulletin of Volcanology*, *69*(7), 811-815.

Coats, R., Kendrick, J.E., Wallace, P.A., Miwa, T., Hornby, A.J., Ashworth, J.D., Matsushima, T. and Lavallée, Y. (2018). Failure criteria for porous dome rocks and lavas: a study of Mt. Unzen, Japan. Solid Earth Discuss, https://doi.org/10.5194/se-2018-19.

Cole, P. D., Calder, E. S., Druitt, T. H., Hoblitt, R., Robertson, R., Sparks, R. S. J., & Young, S. R. (1998). Pyroclastic flows generated by gravitational instability of the 1996–97 lava dome of Soufriere Hills Volcano, Montserrat. *Geophysical Research Letters*, *25*(18), 3425-3428.

Colombier, M., Wadsworth, F. B., Gurioli, L., Scheu, B., Kueppers, U., Di Muro, A., & Dingwell, D. B. (2017). The evolution of pore connectivity in volcanic rocks. *Earth and Planetary Science Letters*, *462*, 99-109.

Cooper, H. W., & Simmons, G. (1977). The effect of cracks on the thermal expansion of rocks. *Earth and Planetary Science Letters*, *36*(3), 404-412.

Cordonnier, B., Hess, K. U., Lavallée, Y., & Dingwell, D. B. (2009). Rheological properties of dome lavas: Case study of Unzen volcano. *Earth and Planetary Science Letters*, *279*(3-4), 263-272.

David, C., Menéndez, B., & Darot, M. (1999). Influence of stress-induced and thermal cracking on physical properties and microstructure of La Peyratte granite. *International Journal of Rock Mechanics and Mining Sciences*, *36*(4), 433-448.

David, E. C., Brantut, N., Schubnel, A., & Zimmerman, R. W. (2012). Sliding crack model for nonlinearity and hysteresis in the uniaxial stress–strain curve of rock. *International Journal of Rock Mechanics and Mining Sciences*, *52*, 9-17.

Dehn, J., Dean, K., & Engle, K. (2000). Thermal monitoring of North Pacific volcanoes from space. *Geology*, *28*(8), 755-758.

del Potro, R., & Hürlimann, M. (2008). Geotechnical classification and characterisation of materials for stability analyses of large volcanic slopes. *Engineering Geology*, *98*(1-2), 1-17.

Duclos, R., & Paquet, J. (1991). High-temperature behaviour of basalts—role of temperature and strain rate on compressive strength and KIc toughness of partially glassy basalts at atmospheric pressure. In *International Journal of Rock Mechanics and Mining Sciences & Geomechanics Abstracts*, 28, 71-76.

Eberhardt, E. (2012). The Hoek-Brown failure criterion. In *The ISRM Suggested Methods for Rock Characterization, Testing and Monitoring: 2007-2014* (pp. 233-240). Springer, Cham.

Eggertsson, G. H., Lavallée, Y., Kendrick, J. E., & Markússon, S. H. (2018). Improving fluid flow in geothermal reservoirs by thermal and mechanical stimulation: The case of Krafla volcano, Iceland. *Journal of Volcanology and Geothermal Research*.

Elsworth, D., Voight, B., Thompson, G., & Young, S. R. (2004). Thermal-hydrologic mechanism for rainfall-triggered collapse of lava domes. *Geology*, *32*(11), 969-972.

Farquharson, J., Heap, M. J., Varley, N. R., Baud, P., & Reuschlé, T. (2015). Permeability and porosity relationships of edifice-forming andesites: a combined field and laboratory study. *Journal of Volcanology and Geothermal Research*, *297*, 52-68.

Farquharson, J. I., Heap, M. J., & Baud, P. (2016a). Strain-induced permeability increase in volcanic rock. *Geophysical Research Letters*, *43*(22).

Farquharson, J. I., Heap, M. J., Lavallée, Y., Varley, N. R., & Baud, P. (2016b). Evidence for the development of permeability anisotropy in lava domes and volcanic conduits. Journal of Volcanology and Geothermal Research, 323, 163-185.

Fredrich, J. T., & Wong, T. F. (1986). Micromechanics of thermally induced cracking in three crustal rocks. *Journal of Geophysical Research: Solid Earth*, *91*(B12), 12743-12764.

Griffiths, L., Heap, M. J., Baud, P., & Schmittbuhl, J. (2017). Quantification of microcrack characteristics and implications for stiffness and strength of granite. *International Journal of Rock Mechanics and Mining Sciences*, *100*, 138-150.

Griffiths, L., Lengliné, O., Heap, M. J., Baud, P., & Schmittbuhl, J. (2018). Thermal cracking in Westerly Granite monitored using direct wave velocity, coda wave interferometry, and acoustic emissions. *Journal of Geophysical Research: Solid Earth*, *123*(3), 2246-2261.

Harnett, C. E., Thomas, M. E., Purvance, M. D., & Neuberg, J. (2018). Using a discrete element approach to model lava dome emplacement and collapse. *Journal of Volcanology and Geothermal Research*, *359*, 68-77.

Heap, M. J., Lavallée, Y., Laumann, A., Hess, K. U., Meredith, P. G., & Dingwell, D. B. (2012). How tough is tuff in the event of fire?. *Geology*, *40*(4), 311-314.

Heap, M. J., Lavallée, Y., Petrakova, L., Baud, P., Reuschlé, T., Varley, N. R., & Dingwell, D. B. (2014). Microstructural controls on the physical and mechanical properties of edifice-forming andesites at Volcán de Colima, Mexico. *Journal of Geophysical Research: Solid Earth*, *119*(4), 2925-2963.

Heap, M. J., Farquharson, J. I., Baud, P., Lavallée, Y., & Reuschlé, T. (2015). Fracture and compaction of andesite in a volcanic edifice. *Bulletin of volcanology*, *77*(6), 55.

Heap, M. J., & Kennedy, B. M. (2016). Exploring the scale-dependent permeability of fractured andesite. *Earth and Planetary Science Letters*, 447, 139-150.

Heap, M. J., Violay, M., Wadsworth, F. B., & Vasseur, J. (2017a). From rock to magma and back again: The evolution of temperature and deformation mechanism in conduit margin zones. *Earth and Planetary Science Letters*, *463*, 92-100.

Heap, M. J., Kushnir, A. R., Gilg, H. A., Wadsworth, F. B., Reuschlé, T., & Baud, P. (2017b). Microstructural and petrophysical properties of the Permo-Triassic sandstones (Buntsandstein) from the Soultz-sous-Forêts geothermal site (France). *Geothermal Energy*, *5*(1), 26.

Heap, M.J., Kushnir, A., Griffiths, L., Wadsworth, F., Marmoni, G.M., Fiorucci, M., Martino, S., Baud, P., Gilg, H.A. and Reuschlé, T. (2018). Fire resistance of the Mt. Epomeo Green Tuff, a widely-used building stone on Ischia Island (Italy). *Volcanica*, *1*(1), 33-48.

Hoek, E., & Brown, E. T. (1997). Practical estimates of rock mass strength. *International Journal of Rock Mechanics and Mining Sciences*, *34*(8), 1165-1186.

Hoek, E., Carranza-Torres, C., & Corkum, B. (2002). Hoek-Brown failure criterion-2002 edition. *Proceedings of NARMS-Tac*, *1*, 267-273.

Hoek, E., & Bieniawski, Z. T. (1965). Brittle fracture propagation in rock under compression. *International Journal of Fracture Mechanics*, *1*(3), 137-155.

Homand-Etienne, F., & Houpert, R. (1989). Thermally induced microcracking in granites: characterization and analysis. In *International Journal of Rock Mechanics and Mining Sciences & Geomechanics Abstracts*, 26, 125-134.

Hutchison, W., Varley, N., Pyle, D. M., Mather, T. A., & Stevenson, J. A. (2013). Airborne thermal remote sensing of the Volcán de Colima (Mexico) lava dome from 2007 to 2010. *Geological Society, London, Special Publications*, *380*(1), 203-228.

James, M. R., & Varley, N. (2012). Identification of structural controls in an active lava dome with high resolution DEMs: Volcán de Colima, Mexico. *Geophysical Research Letters*, *39*(22).

Kaneko, T., Wooster, M. J., & Nakada, S. (2002). Exogenous and endogenous growth of the Unzen lava dome examined by satellite infrared image analysis. *Journal of Volcanology and Geothermal Research*, *116*(1-2), 151-160.

Kendrick, J. E., Smith, R., Sammonds, P., Meredith, P. G., Dainty, M., & Pallister, J. S. (2013). The influence of thermal and cyclic stressing on the strength of rocks from Mount St. Helens, Washington. *Bulletin of Volcanology*, *75*(7), 728.

Kendrick, J. E., Lavallée, Y., Varley, N. R., Wadsworth, F. B., Lamb, O. D., & Vasseur, J. (2016). Blowing off steam: tuffisite formation as a regulator for lava dome eruptions. *Frontiers in Earth Science*, *4*, 41.

Kolzenburg, S., Heap, M., Lavallée, Y., Russell, J., Meredith, P., & Dingwell, D. B. (2012). Strength and permeability recovery of tuffisite-bearing andesite. *Solid Earth*, *3*, 191-198.

Kushnir, A. R., Martel, C., Bourdier, J. L., Heap, M. J., Reuschlé, T., Erdmann, S., ... & Cholik, N. (2016). Probing permeability and microstructure: Unravelling the role of a low-permeability dome on the explosivity of Merapi (Indonesia). *Journal of Volcanology and Geothermal Research*, *316*, 56-71.

Kranz, R. L. (1983). Microcracks in rocks: a review. *Tectonophysics*, *100*(1-3), 449-480.

Lamur, A., Lavallée, Y., Iddon, F. E., Hornby, A. J., Kendrick, J. E., Aulock, F. W., & Wadsworth, F. B. (2018). Disclosing the temperature of columnar jointing in lavas. *Nature Communications*, *9*(1), 1432.

Lavallée, Y., Hess, K. U., Cordonnier, B., & Bruce Dingwell, D. (2007). Non-Newtonian rheological law for highly crystalline dome lavas. *Geology*, *35*(9), 843-846.

Lavallée, Y., Varley, N.R., Alatorre-Ibargüengoitia, M.A., Hess, K.U., Kueppers, U., Mueller, S., Richard, D., Scheu, B., Spieler, O. and Dingwell, D.B. (2012). Magmatic architecture of dome-building eruptions at Volcán de Colima, Mexico. *Bulletin of Volcanology*, *74*(1), 249-260.

Lavallée, Y., Benson, P.M., Heap, M.J., Hess, K.U., Flaws, A., Schillinger, B., Meredith, P.G. and Dingwell, D.B. (2013). Reconstructing magma failure and the degassing network of dome-building eruptions. *Geology*, *41*(4), 515-518.

Loaiza, S., Fortin, J., Schubnel, A., Guéguen, Y., Vinciguerra, S., & Moreira, M. (2012). Mechanical behavior and localized failure modes in a porous basalt from the Azores. *Geophysical Research Letters*, *39*(19).

Loughlin, S.C., Luckett, R., Ryan, G., Christopher, T., Hards, V., De Angelis, S., Jones, L. and Strutt, M. (2010). An overview of lava dome evolution, dome collapse and cyclicity at Soufrière Hills Volcano, Montserrat, 2005–2007. *Geophysical Research Letters*, *37*(19).

667 Marinos, V. I. I. I., Marinos, P., & Hoek, E. (2005). The geological strength index:
668 applications and limitations. *Bulletin of Engineering Geology and the*
669 *Environment*, *64*(1), 55-65.
670 Matthews, A. J., & Barclay, J. (2004). A thermodynamical model for rainfall-triggered
671 volcanic dome collapse. *Geophysical Research Letters*, *31*(5).
672 Moon, V., Bradshaw, J., Smith, R., & de Lange, W. (2005). Geotechnical characterisation of
673 stratocone crater wall sequences, White Island Volcano, New Zealand. *Engineering*
674 *geology*, *81*(2), 146-178.
675 Mueller, S. B., Varley, N. R., Kueppers, U., Lesage, P., Reyes-Dávila, G., & Dingwell, D. B.
676 (2013). Quantification of magma ascent rate through rockfall monitoring at the
677 growing/collapsing lava dome of Volcán de Colima, Mexico. *Solid Earth*, *4*, 201-
678 213.
679 Ogburn, S. E., Loughlin, S. C., & Calder, E. S. (2015). The association of lava dome growth
680 with major explosive activity (VEI≥ 4): DomeHaz, a global dataset. Bulletin of
681 Volcanology, 77(5), 40.
682 Okubo, C. H. (2004). Rock mass strength and slope stability of the Hilina slump, Kīlauea
683 volcano, Hawai'i. *Journal of Volcanology and Geothermal Research*, *138*(1-2), 43-76.
684 Oppenheimer, C., Francis, P. W., Rothery, D. A., Carlton, R. W., & Glaze, L. S. (1993).
685 Infrared image analysis of volcanic thermal features: Lascar Volcano, Chile, 1984–
686 1992. *Journal of Geophysical Research: Solid Earth*, *98*(B3), 4269-4286.
687 Richter, D., & Simmons, G. (1974). Thermal expansion behavior of igneous rocks.
688 In *International Journal of Rock Mechanics and Mining Sciences & Geomechanics*
689 *Abstracts*, 11, 403-411.
690 Rosas-Carbajal, M., Komorowski, J. C., Nicollin, F., & Gibert, D. (2016). Volcano electrical
691 tomography unveils edifice collapse hazard linked to hydrothermal system
692 structure and dynamics. *Scientific Reports*, *6*, 29899.
693 Ryan, A. G., Friedlander, E. A., Russell, J. K., Heap, M. J., & Kennedy, L. A. (2018). Hot
694 pressing in conduit faults during lava dome extrusion: Insights from Mount St.
695 Helens 2004–2008. *Earth and Planetary Science Letters*, *482*, 171-180.
696 Sahetapy-Engel, S. T., Harris, A. J., & Marchetti, E. (2008). Thermal, seismic and
697 infrasound observations of persistent explosive activity and conduit dynamics at
698 Santiaguito lava dome, Guatemala. *Journal of Volcanology and Geothermal*
699 *Research*, *173*(1-2), 1-14.
700 Sahetapy-Engel, S. T., & Harris, A. J. (2009). Thermal structure and heat loss at the
701 summit crater of an active lava dome. *Bulletin of Volcanology*, *71*(1), 15-28.
702 Schaefer, L. N., Kendrick, J. E., Oommen, T., Lavallée, Y., & Chigna, G. (2015).
703 Geomechanical rock properties of a basaltic volcano. *Frontiers in Earth Science*, *3*,
704 29.
705 Scholz, C. H. (1968). Microfracturing and the inelastic deformation of rock in
706 compression. *Journal of Geophysical Research*, *73*(4), 1417-1432.
707 Shea, T., Houghton, B. F., Gurioli, L., Cashman, K. V., Hammer, J. E., & Hobden, B. J. (2010).
708 Textural studies of vesicles in volcanic rocks: an integrated methodology. *Journal*
709 *of Volcanology and Geothermal Research*, *190*(3-4), 271-289.
710 Siratovich, P. A., Villeneuve, M. C., Cole, J. W., Kennedy, B. M., & Bégué, F. (2015).
711 Saturated heating and quenching of three crustal rocks and implications for
712 thermal stimulation of permeability in geothermal reservoirs. *International*
713 *Journal of Rock Mechanics and Mining Sciences*, *80*, 265-280.

Sparks, R. S. J. (1997). Causes and consequences of pressurisation in lava dome eruptions. *Earth and Planetary Science Letters*, *150*(3-4), 177-189.

Smellie, J. L., Millar, I. L., Rex, D. C., & Butterworth, P. J. (1998). Subaqueous, basaltic lava dome and carapace breccia on King George island, South Shetland Islands, Antarctica. *Bulletin of Volcanology*, *59*(4), 245-261.

Smith, R., Sammonds, P. R., & Kilburn, C. R. (2009). Fracturing of volcanic systems: experimental insights into pre-eruptive conditions. *Earth and Planetary Science Letters*, *280*(1-4), 211-219.

Smith, R., Sammonds, P. R., Tuffen, H., & Meredith, P. G. (2011). Evolution of the mechanics of the 2004–2008 Mt. St. Helens lava dome with time and temperature. *Earth and Planetary Science Letters*, *307*(1-2), 191-200.

Stevenson, J. A., & Varley, N. (2008). Fumarole monitoring with a handheld infrared camera: Volcán de Colima, Mexico, 2006–2007. *Journal of Volcanology and Geothermal Research*, *177*(4), 911-924.

Thomas, M. E., Petford, N., & Bromhead, E. N. (2004). Volcanic rock-mass properties from Snowdonia and Tenerife: implications for volcano edifice strength. *Journal of the Geological Society*, *161*(6), 939-946.

Varley, N., Connor, C., & Komorowski, J.-C. (2018). Volcán de Colima: Managing the Threat. Springer-Verlag Berlin Heidelberg.

Vinciguerra, S., Trovato, C., Meredith, P. G., & Benson, P. M. (2005). Relating seismic velocities, thermal cracking and permeability in Mt. Etna and Iceland basalts. *International Journal of Rock Mechanics and Mining Sciences*, *42*(7-8), 900-910.

Voight, B., & Elsworth, D. (2000). Instability and collapse of hazardous gas-pressurized lava domes. *Geophysical Research Letters*, *27*(1), 1-4.

Voight, B. (2000). Structural stability of andesite volcanoes and lava domes. *Philosophical Transactions of the Royal Society of London A: Mathematical, Physical and Engineering Sciences*, *358*(1770), 1663-1703.

Voight, B., Linde, A.T., Sacks, I.S., Mattioli, G.S., Sparks, R.S.J., Elsworth, D., Hidayat, D., Malin, P.E., Shalev, E., Widiwijayanti, C. and Young, S.R. (2006). Unprecedented pressure increase in deep magma reservoir triggered by lava-dome collapse. *Geophysical Research Letters*, *33*(3).

Watts, R. B., Herd, R. A., Sparks, R. S. J., & Young, S. R. (2002). Growth patterns and emplacement of the andesitic lava dome at Soufriere Hills Volcano, Montserrat. *Geological Society, London, Memoirs*, *21*(1), 115-152.

Watters, R. J., Zimbelman, D. R., Bowman, S. D., & Crowley, J. K. (2000). Rock mass strength assessment and significance to edifice stability, Mount Rainier and Mount Hood, Cascade Range volcanoes. *Pure and Applied Geophysics*, *157*(6-8), 957-976.

Wooster, M. J., & Kaneko, T. (1998). Satellite thermal analyses of lava dome effusion rates at Unzen Volcano, Japan. *Journal of Geophysical Research: Solid Earth*, *103*(B9), 20935-20947.

Yong, C., & Wang, C. Y. (1980). Thermally induced acoustic emission in Westerly granite. *Geophysical Research Letters*, *7*(12), 1089-1092.

Zhu, W., Baud, P., Vinciguerra, S., & Wong, T. F. (2016). Micromechanics of brittle faulting and cataclastic flow in Mount Etna basalt. *Journal of Geophysical Research: Solid Earth*, *121*(6), 4268-4289.

760 Zorn, E. U., Rowe, M. C., Cronin, S. J., Ryan, A. G., Kennedy, L. A., & Russell, J. K. (2018).
761 Influence of porosity and groundmass crystallinity on dome rock strength: a case
762 study from Mt. Taranaki, New Zealand. *Bulletin of Volcanology*, *80*(4), 35.
763

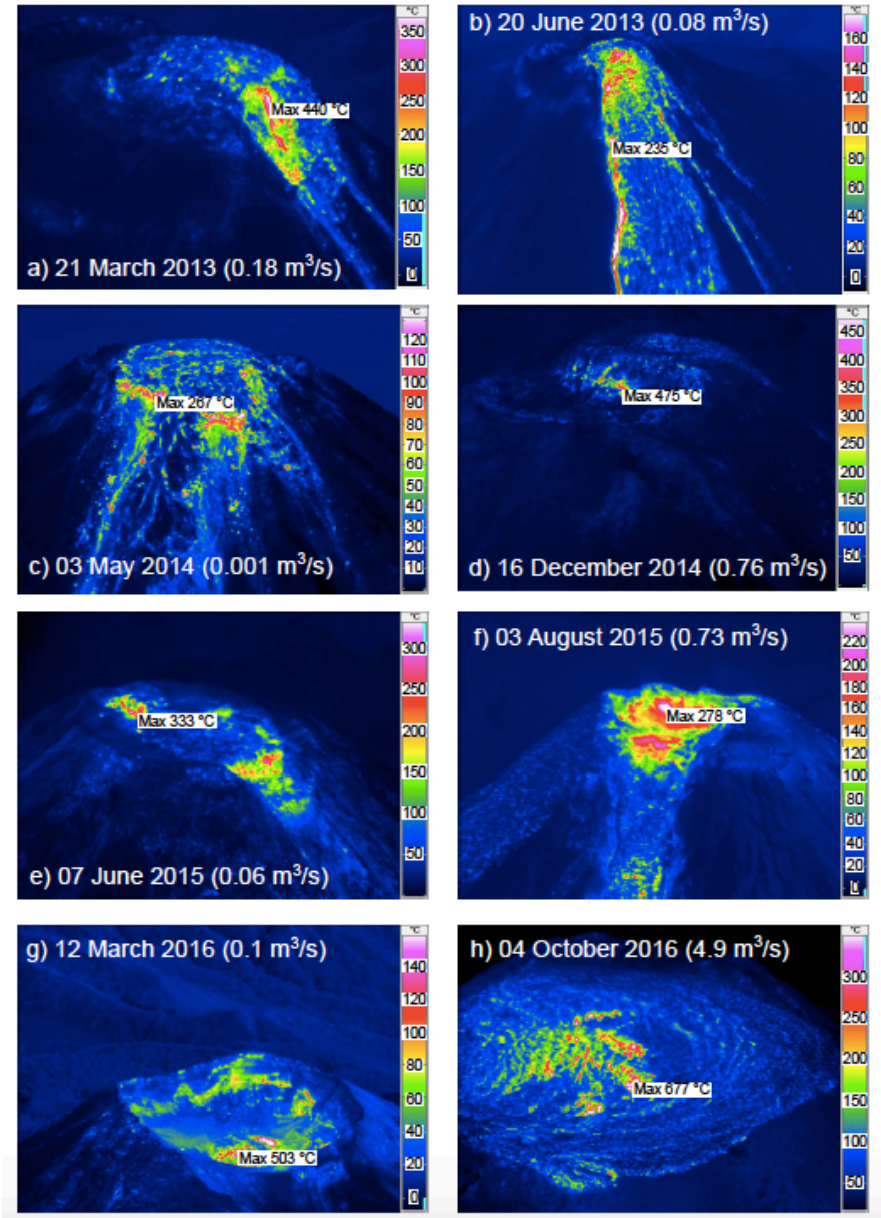

764

765 **Figure 1.** Airborne thermal images of the dome at Volcán de Colima (Mexico) taken
766 using a Jenoptic VarioCAMHR thermal camera (see Hutchinson et al. (2013) for technical
767 specifications). (a) 21 March 2013 – slow dome growth with overflow to lava flow. (b)
768 20 June 2013 – slow lava extrusion with overflow to long lava flow. (c) 03 May 2014 –
769 revitalised dome growth with higher effusion rate. (d) 16 December 2014 – post-
770 subsidence growth of a new lobe. (e) 07 June 2015 – dome growth from two effusion
771 centres. (f) 03 August 2015 – post-eruption emplacement of a new lava dome. (g) 12
772 March 2016 – post-eruption and subsidence. (h) 04 October 2016 – fast-growing flat-
773 topped dome. The corresponding extrusion rates are indicated on each of the images.

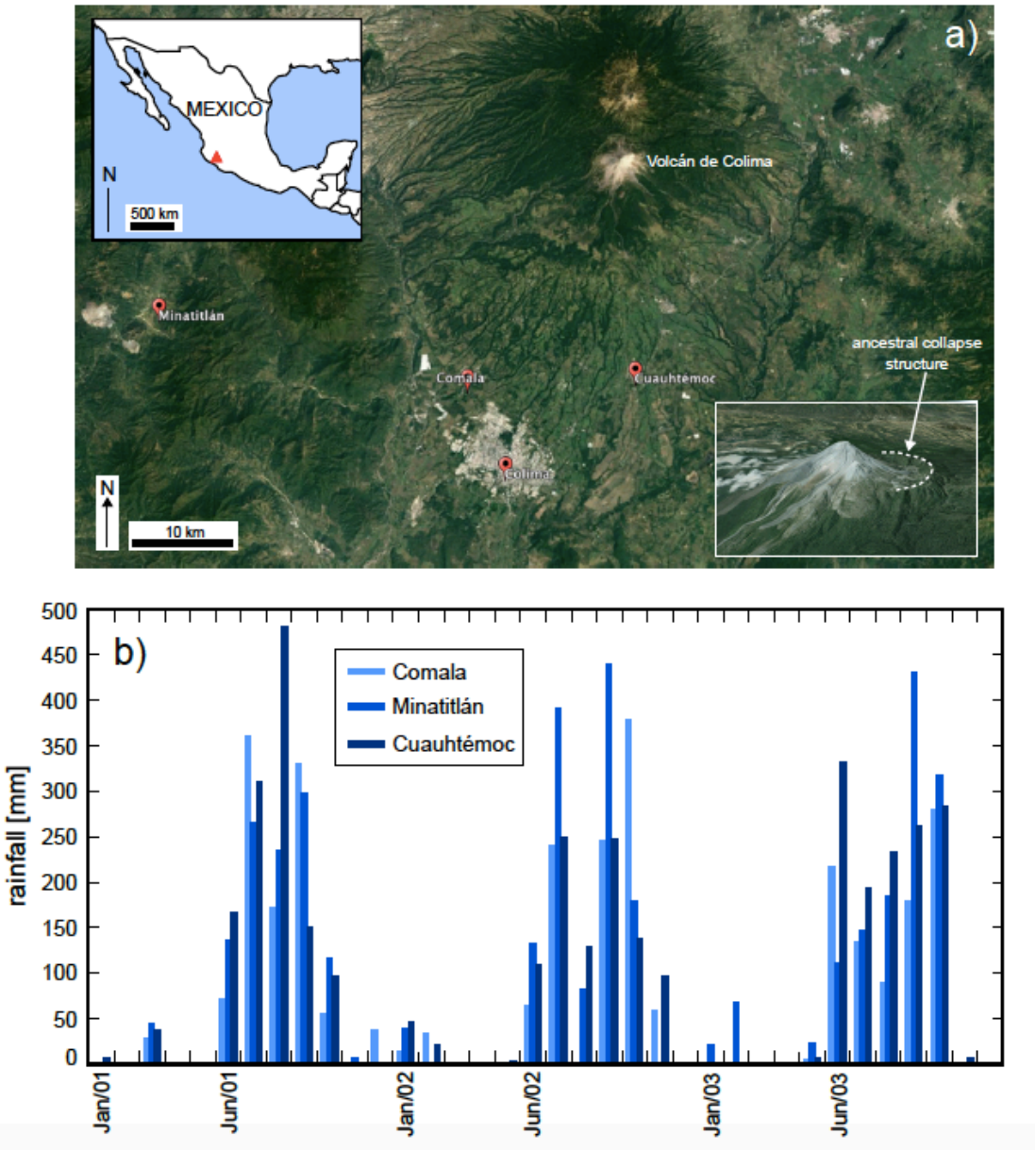

774

775 **Figure 2.** (a) Map showing the location of Volcán de Colima (Google Earth). Insets show
776 a map of Mexico showing the location of Volcán de Colima (the red triangle) and an
777 image showing the ancestral collapse structure at Volcán de Colima (Google Earth). (b)
778 Rainfall data (from January 2001 to December 2003) obtained from permanent
779 meteorological monitoring stations that form part of the CONAGUA (Comisión Nacional
780 del Agua) network. Three stations were chosen: the towns of Cuauhtémoc, Comala, and
781 Minatitlán (see panel (a) for town locations). These towns are at a distance of 19, 24,
782 and 46 km from the vent of the volcano, respectively (Figure 2a).

783

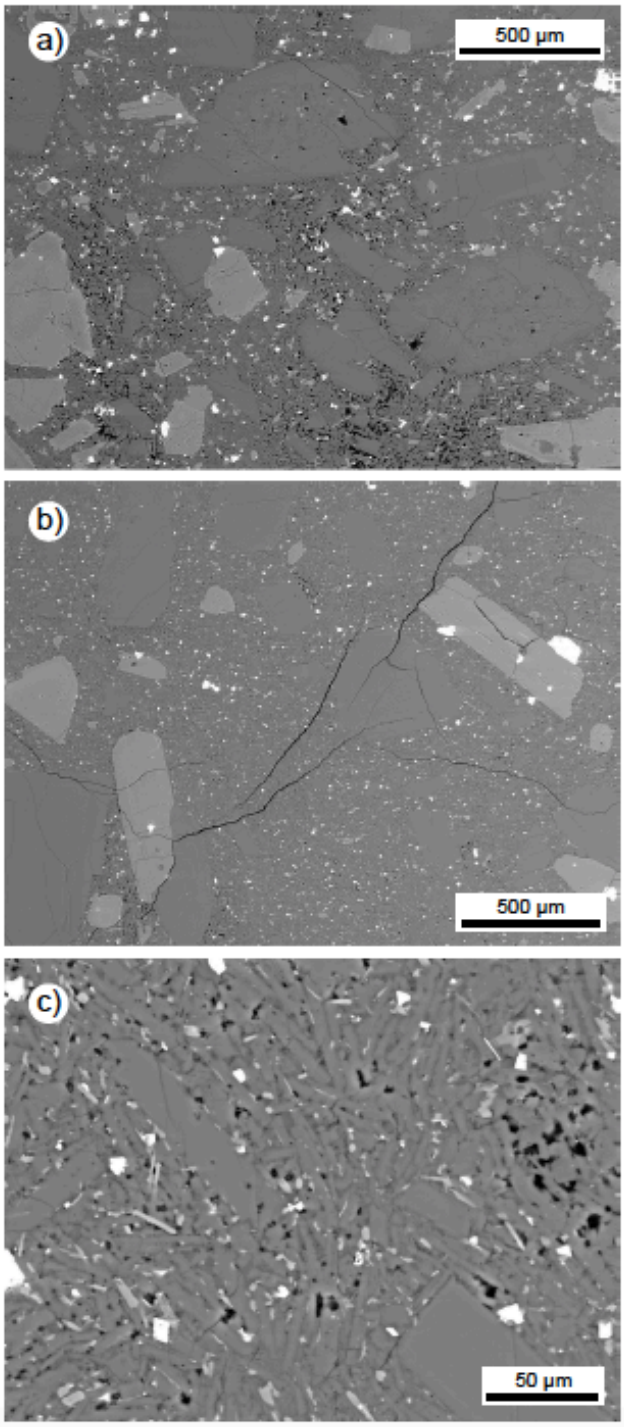

784

785 **Figure 3.** Backscattered scanning electron microscope (BSE) images of the andesite
786 used in this study. (a) BSE image showing the porphyritic texture (phenocrysts and
787 groundmass) and the nature of the diktytaxitic porosity (pores appear as black). (b) BSE
788 image showing the microcracks present within the as-collected material. (c) BSE image
789 showing the crystallised nature of the groundmass. Porosity (in black) can also be seen
790 as the gaps between certain microlites.

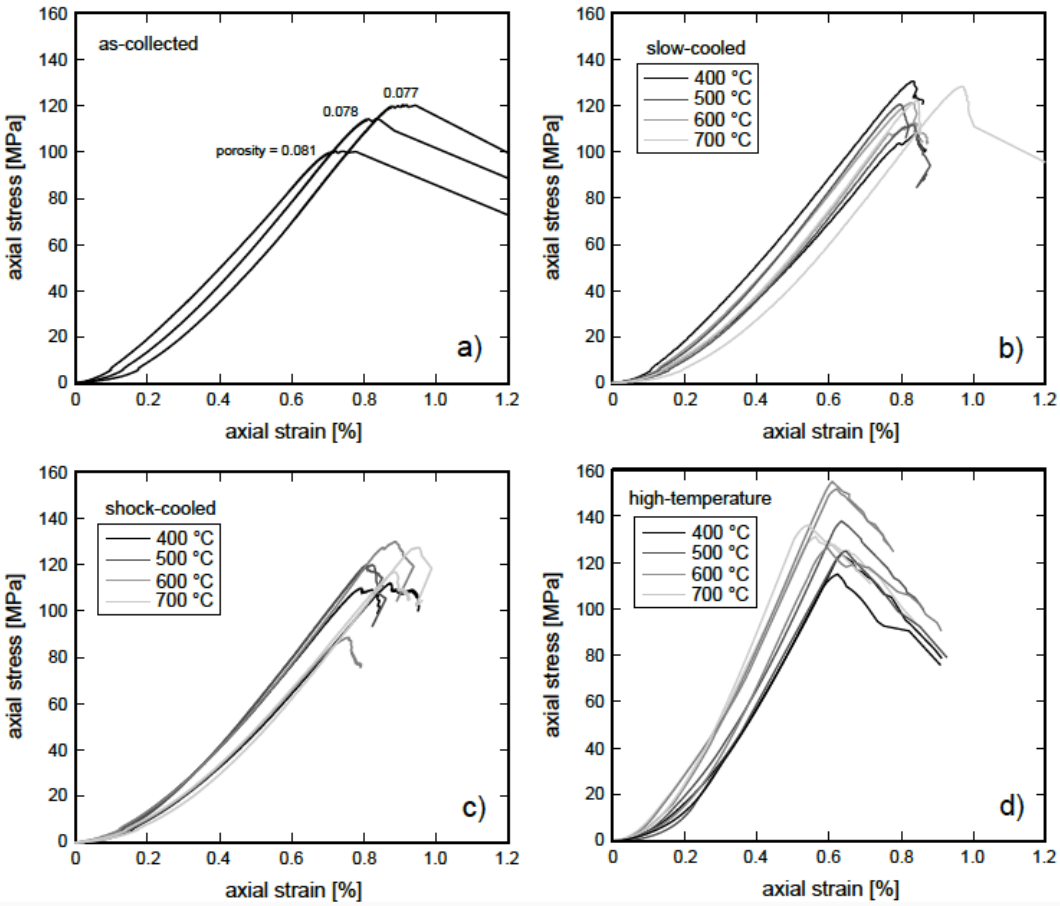

791

792 **Figure 4**. (a) Stress-strain curves for three as-collected samples with different
793 porosities (the porosity of the sample is indicated next to each curve). (b) Stress-strain
794 curves for the eight slow-cooled samples. (c) Stress-strain curves for the eight shock-
795 cooled samples. (d) Stress-strain curves for the eight samples deformed at high in-situ
796 temperatures.

797

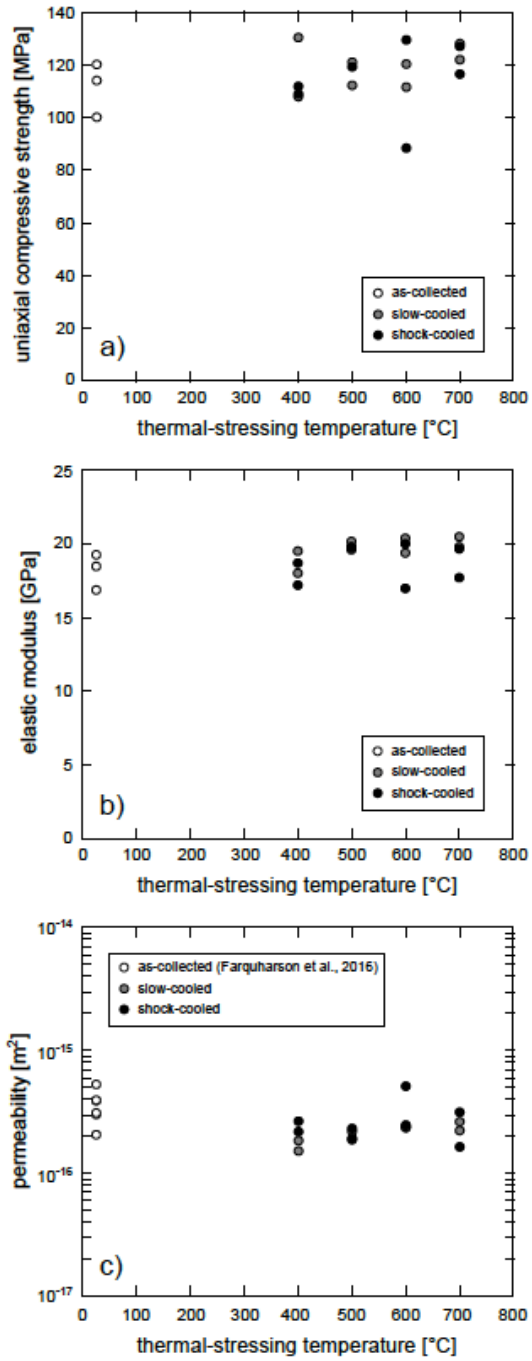

798

799 **Figure 5.** Physical property measurements on as-collected, slow-, and shock-cooled
800 samples of andesite. (a) Uniaxial compressive strength as a function of thermal-stressing
801 temperature. (b) Elastic modulus as a function of thermal-stressing temperature. (c)
802 Permeability as a function of thermal-stressing temperature. The permeability of the as-
803 collected samples was taken from Farquharson et al. (2016a). The data unique to this
804 study are available in Table 1.

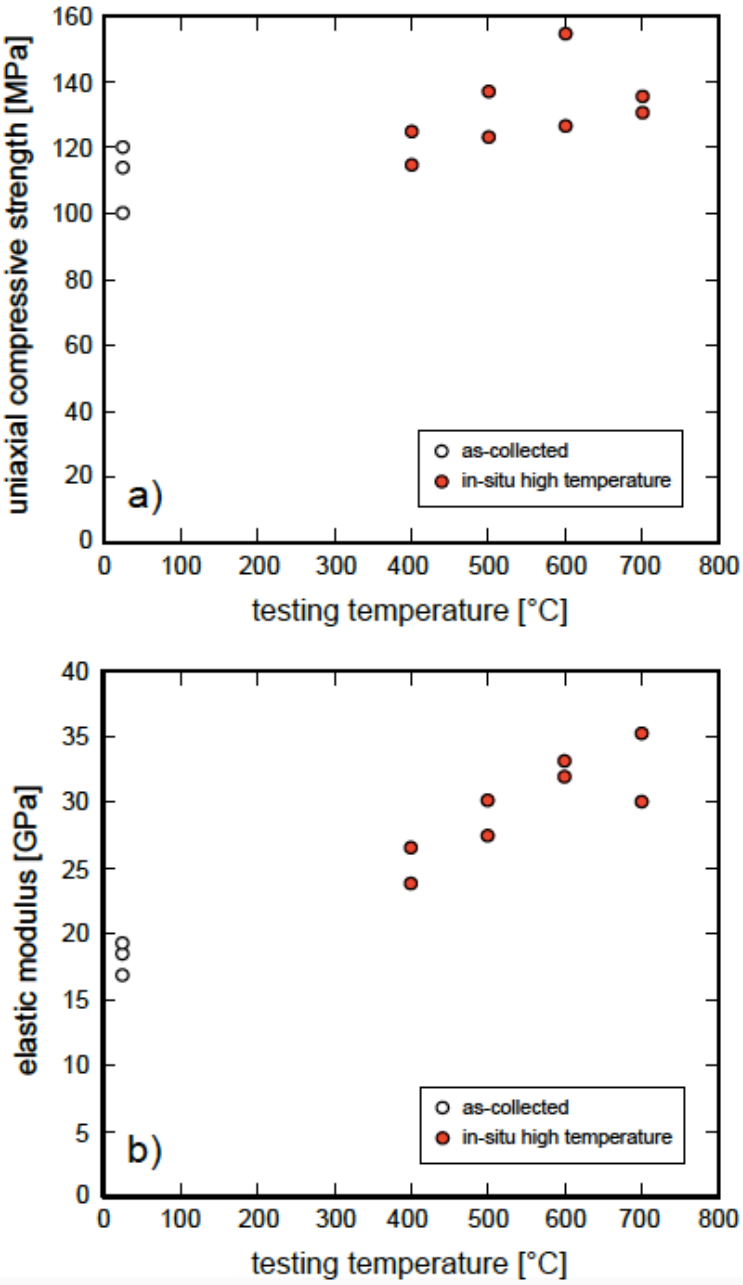

805

806 **Figure 6.** Uniaxial compressive strength (a) and elastic modulus (b) of the andesite as a

807 function of testing temperature. The data are available in Table 2.

808

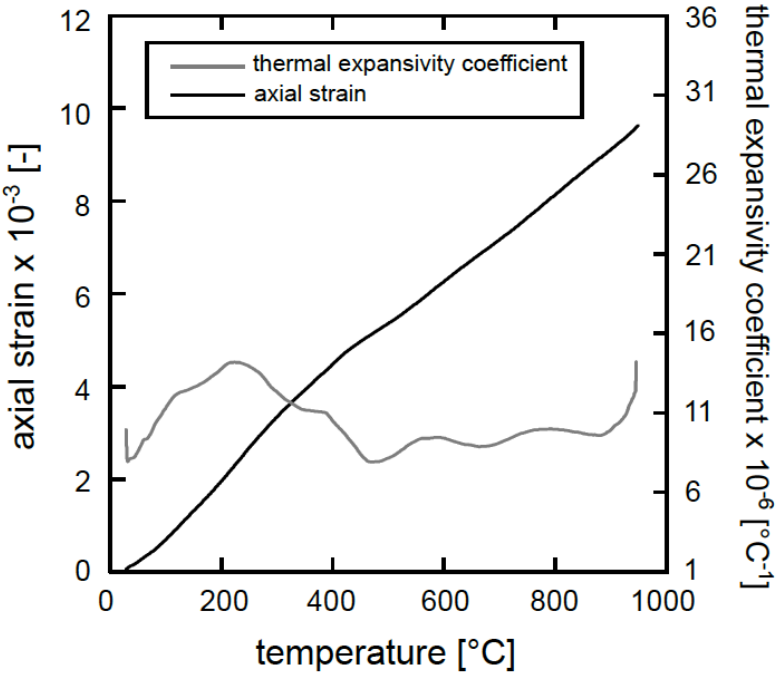

809

810 **Figure 7.** Axial strain (black line) and thermal expansivity coefficient (grey line) as a
811 function of temperature for the andesite studied, as measured by a Netzsch TMA 402 F1
812 Hyperion Thermo-mechanical Analyser (TMA). Note: the increase in thermal
813 expansivity below 200 °C is an artefact related to the heating program.

814

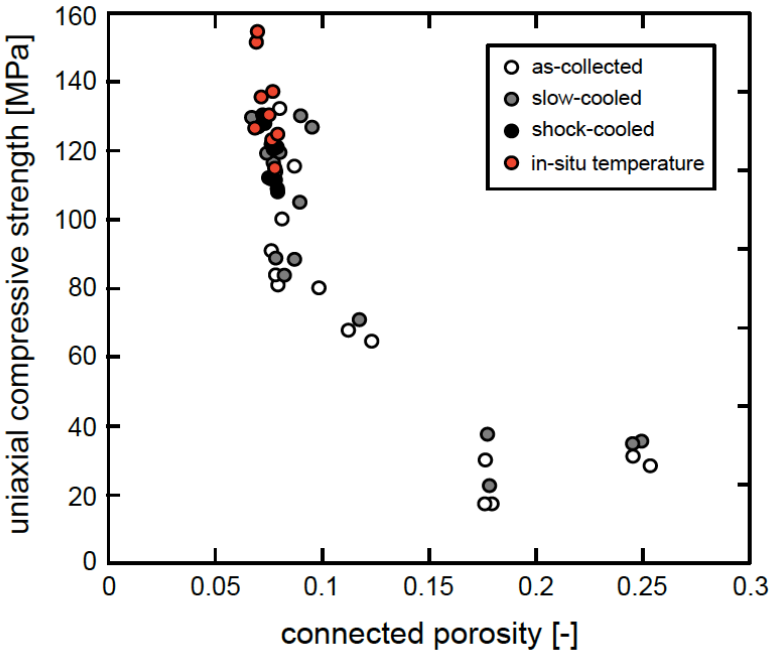

815

816 **Figure 8.** Uniaxial compressive strength as a function of connected porosity for
817 andesites from Volcán de Colima. As-collected data from this study and Heap et al.
818 (2014; 2015), slow-cooled (400-700 °C) data from this study and Heap et al. (2014),
819 shock-cooled (400-700 °C) and high in-situ temperature (400-700 °C) data and from
820 this study. The data unique to this study are available in Tables 1 and 2.

821 **Table 1**. Summary of the data collected for the as-collected and thermally-stressed
822 andesite samples. Permeability measured under a confining pressure of 1 MPa (see text
823 for details).
824

Sample	Initial connected porosity	Thermal-stressing temperature (°C)	Cooling method	Connected porosity following thermal-stressing	Permeability following thermal stressing (m^2)	Uniaxial compressive strength (MPa)	Elastic modulus (GPa)
EZ-1	0.078	-	-	-	-	114.1	18.5
EZ-2	0.077	-	-	-	-	120.2	19.3
EZ-3	0.081	-	-	-	-	100.2	16.9
EZ-4	0.076	400	shock	0.077	2.66×10^{-16}	111.9	17.2
EZ-7	0.079	400	shock	0.085	2.18×10^{-16}	109.0	18.7
EZ-14	0.072	400	slow	0.091	1.51×10^{-16}	130.4	19.5
EZ-15	0.079	400	slow	0.067	1.85×10^{-16}	108.0	18.0
EZ-8	0.080	500	shock	0.082	1.91×10^{-16}	119.6	19.7
EZ-9	0.074	500	shock	0.076	2.32×10^{-16}	119.4	19.8
EZ-16	0.079	500	slow	0.081	1.88×10^{-16}	121.1	19.6
EZ-17	0.075	500	slow	0.077	2.18×10^{-16}	112.2	20.2
EZ-10	0.087	600	shock	0.074	5.10×10^{-16}	88.5	17.0
EZ-11	0.067	600	shock	0.076	2.46×10^{-16}	129.7	20.0
EZ-12	0.078	600	slow	0.078	2.33×10^{-16}	111.6	19.4
EZ-13	0.077	600	slow	0.078	2.39×10^{-16}	120.4	20.4
EZ-5	0.077	700	shock	0.079	3.15×10^{-16}	116.6	17.7
EZ-6	0.070	700	shock	0.073	1.64×10^{-16}	127.1	19.7
EZ-18	0.076	700	slow	0.074	2.61×10^{-16}	122.0	20.5
EZ-19	0.073	700	slow	0.074	2.25×10^{-16}	128.1	19.8

825

826 **Table 2**. Summary of the high *in-situ* temperature uniaxial compressive strength tests.

827

Sample	Initial connected porosity	Temperature (°C)	Uniaxial compressive strength (MPa)	Elastic modulus (GPa)
EZ-22	0.078	400	114.9	26.6
EZ-23	0.079	400	124.9	23.9
EZ-24	0.077	500	137.2	30.2
EZ-25	0.076	500	123.2	27.5
EZ-26	0.069	600	151.6	31.7
EZ-27	0.070	600	154.8	33.2
EZ-28	0.068	600	126.6	32.0
EZ-21	0.075	700	130.6	30.1
EZ-29	0.071	700	135.7	35.2

828